LOWLAND TECHNOLOGY INTERNATIONAL Vol. 4, No. 2, 14-24, December 2002
International Association of Lowland Technology (IALT), ISSN 1344-9656

THE INFLUENCE OF INITIAL STATIC SHEAR STRESS ON POST-CYCLIC DEGRADATION OF NON-PLASTIC SILT

B.- W. Song[1]

ABSTRACT: Using a sequential procedure of cyclic and post-cyclic direct simple shear (DSS) tests, the strength and stiffness degradation characteristics of non-plastic silt were studied during and immediately after cyclic loading. The post-cyclic degradations of strength and stiffness were considered with special reference to the effects of initial static shear stress (ISSS). The findings obtained from sequential DSS testing on non-plastic silt are: (1) strength and stiffness degradation characteristics of non-plastic silt during post-cyclic loading depend on the increase of the normalized pore pressures generated during cyclic loading, which is more marked with increasing ISSS; (2) degradation of stiffness is particularly to ISSS; (3) post-cyclic degradation relations of strength and stiffness for non-plastic silt formulated against cyclic-induced excess pore pressure should include the influence of ISSS. The methods formulated for predicting post-cyclic strength and stiffness take the effect of ISSS into consideration.

Key words: Non-plastic silt, direct simple shear test, cyclic test, monotonic test, constant volume condition, degradation of strength and stiffness, post-cyclic loading

INTRODUCTION

It has been reported that during recent earthquakes such as the 1999 Turkey Earthquake (JGS 2000a) and the 2000 Tottoriken-Seibu Earthquake (2000b), silty soils liquefaction led to lateral ground flow (Hamada et al. 1999; JGS 2000a; Shimamoto et al. 2001). In both cases, the damaged sites were closed to the river or sea and had very high ground water levels, close to the surface.

For example, the silty ground damaged during the 1999 Turkey Earthquake lies in the region between Adapazari and Sapanca near the mouth of the Sakarya River (Aydan et al. 2000; Hamada et al. 1999; JGS 2000a). The city of Adapazari was founded on an alluvial stratum and consists of residual soils transferred from the river about 200 years ago; its ground is constituted of silty clay and non-plastic silts. The ground water level was only 1~3m below the surface. The 1999 Turkey Earthquake caused a number of structures in Adapazari to be damaged due to liquefaction.

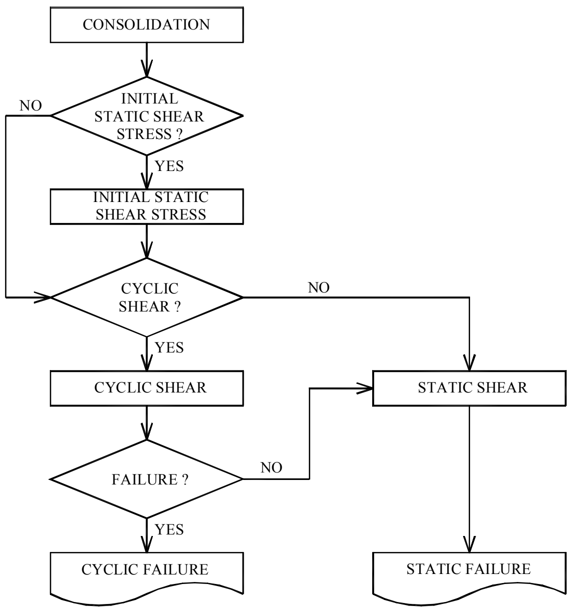

Fig. 1 Procedure for the direct simple shear (DSS) test

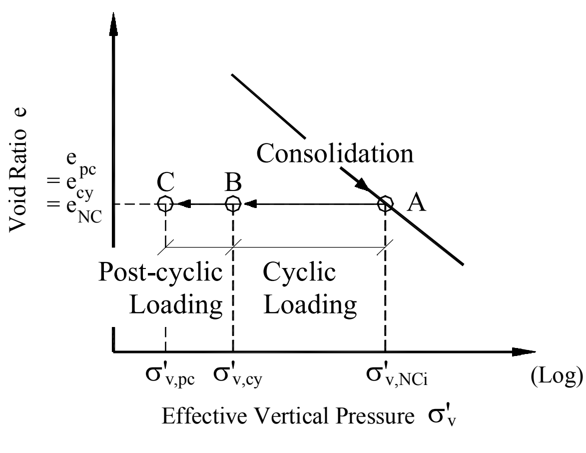

Fig. 2 Soil test state path

1 PhD Candidate, School of Science and Engineering, Ibaraki University, Ibaraki Japan.
Note: Discussion on this paper is open until December 25, 2003.

Many buildings settled, tilted or totally collapsed due to liquefaction of silt or silty sand. Vertical displacement of buildings up to 1.1 m was observed. More typically, buildings suffered severe tilting due to loss of bearing capacity in the foundation ground. Such structural incapacitation was particularly severe along the border between liquefied and non-liquefied areas.

During the 2000 Tottoriken-Seibu Earthquake the most serious damage due to silt liquefaction occurred at the Takenouchi Industrial Complex near seaside (Shimamoto et al. 2001). The non-plastic silt beneath this site had a 2.4 ~ 5.6 uniformity coefficient U_c and was 50~100% fines. Settlement of 0.1 ~ 0.3 m and lateral flow of about 0.2 m were reported there.

This study examines whether silt has a high potential for liquefaction and lateral flow. It also examines how silty soils are affected by ISSS, which is counted as an important issue in relation to the stability of silty soils beneath structures and in sloping ground during earthquakes. The NGI type Direct Simple Shear(DSS) tests (Bjerrum and Landva, 1966) were central in determining the cyclic and post-cyclic degradation of non-plastic silt. Specifically, it is investigated as the following:

1) The degradation of strength and stiffness of non-plastic silt were investigated using DSS tests, and
2) The cyclic strength and stiffness characteristics of non-plastic silt were studied with an emphasis on the effects of ISSS, and
3) Using the results from cyclic DSS tests, it is proposed a method for predicting post-cyclic strength and stiffness taking into consideration for the effect of ISSS.

TESTING PROCEDURE FOR INVESTIGATION OF BOTH CYCLIC AND POST-CYCLIC CHARACTERISTICS

Basic Concept

In previous papers such as those by Yasuhara (Yasuhara et al. 1983, 1992; Yasuhara 1985, 1994a, 1994b), the cyclic triaxial test has been used to investigate changes in strength and stiffness of cohesive soils under cyclic loading conditions. Figure 1 presents the steps in a procedure for obtaining the behaviour of soils both during and after cyclic loading with ISSS τ_s. The procedure shown in Fig. 1 has also been adopted for the simple shear test (Andersen et al. 1976; Vucetic et al. 1998) and the cyclic direct shear test (Yasuhara and Nagano 1995). Cyclic parameters during and after loading are commonly divided into two categories: strength and stiffness. These characteristics depend on the magnitude of cyclically induced pore pressures and shear strains. For this reason, it is investigated that the relation of post-cyclic strength and stiffness characteristics to excess pore pressure in non-plastic silt.

Testing Procedure

Cyclic DSS tests were carried out to investigate post-cyclic degradation of strength and stiffness. In this test, as shown in Fig. 2, a constant specimen height is maintained during both cyclic and post-cyclic loading to hold the constant volume condition.

Specimens were initially consolidated under a vertical effective stress $\sigma'_{v,NCi}$ at point A in Fig. 2. The vertical effective stress $\sigma'_{v,NCi}$ moved to point B ($\sigma'_{v,cy}$) due to the excess pore pressure generated during cyclic loading under constant volume conditions. This means that the difference between the vertical effective stress $\sigma'_{v,NCi}$ after consolidation and the vertical effective stress after cyclic loading $\sigma'_{v,cy}$ should be equal to the excess pore pressure generated by cyclic loading. The ISSS τ_s was applied after pre-consolidation under drained constant stress conditions. Because of applying this ISSS to each specimen, a small change in the void ratio took place. However, it should be noted that the change in the void ratio was negligibly small. To evaluate the post-cyclic degradation of stiffness, a strain-controlled monotonic test was also performed under constant volume conditions after cyclic loading. This is called the "post-cyclic loading process".

NGI TYPE TESTING DEVICE OF DIRECT SIMPLE SHEAR TEST AND BENDER ELEMENT

Figure 3 shows the NGI-type DSS apparatus with the bender element, which has been in use at Ibaraki University. In Fig. 3(a), vertical and horizontal stresses up to 5MPa by air pressure and 2MPa by oil pressure can be applied to each specimen. Vertical and horizontal displacement can be measured up to 10mm using strain gauges. Vertical displacement during preconsolidation and shear tests show the average value of results from two gauges attached at the left and right sides of circular-shaped with 70 mm diameter and 30 mm height. As shown in Fig. 3, gauges 1 and 2 are attached at the top and bottom of pressure plate, respectively, separately for measurement of horizontal displacement. A load or a displacement controller can modulate the rate of vertical and horizontal load. Each specimen is contained in a wire-reinforced membrane. In other words, this NGI-type DSS apparatus is capable of performing tests under the K_0 condition during preconsolidation. The undrained, or constant volume condition is achieved by keeping the height of specimens constant throughout shear testing. Thus, excess pore pressures are determined by the difference between initial

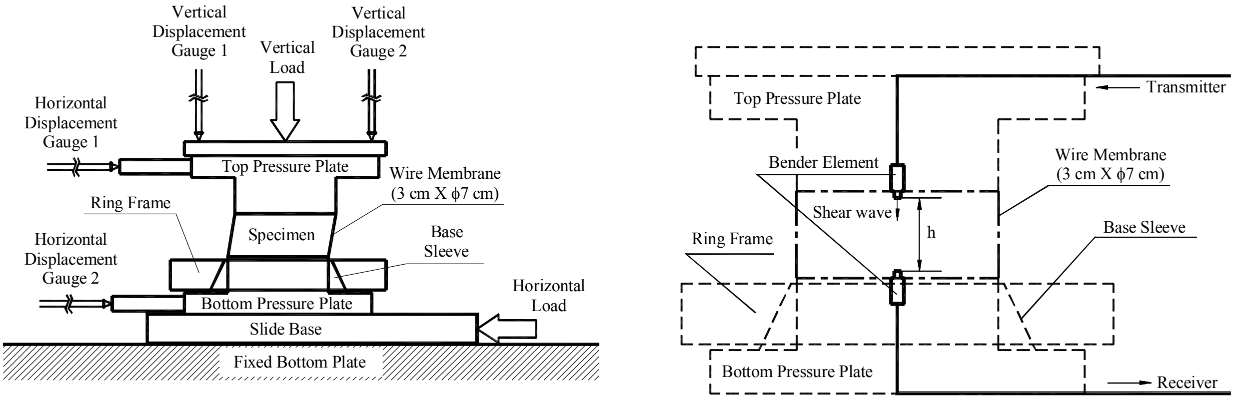

(a) NGI-type DSS testing apparatus (b) Bender element

Fig. 3 Illustration of NGI-type DSS apparatus and bender element

vertical stress and the present vertical stress before and after cyclic shearing, respec

As shown in Fig. the center of the top a measuring the vel consolidation and at shear wave is sent fr (bottom) in this devi DSS tests using the b benchmark for reliabi bender element is use during consolidation b during cyclic test whe

and minimum void ratio e_{max}, e_{min} were 1.47 and 0.71,

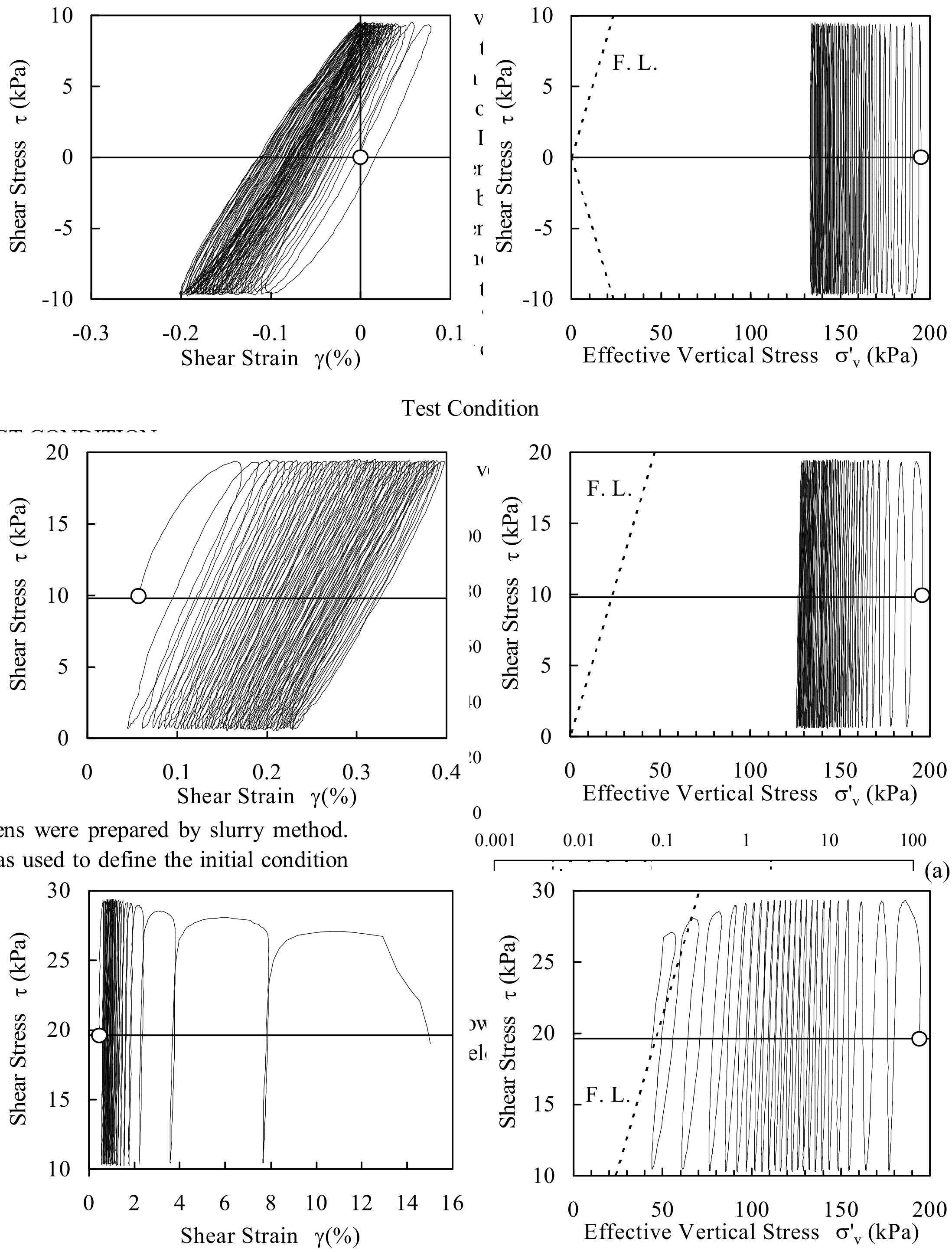

Test Condition

SPECIMEN AND TE

Soil Property and Spe

Grain size distrib shown in Fig. 4. Nor The dotted and the d distribution ranges of respectively (JGS 19 feasibilities, the DL C There is no plasticity i density of soil particl limit w_L was 25.1%.

All of the specimens were prepared by slurry method. Relative density D_r was used to define the initial condition of the specimens. To c to determine the max $\rho_{d,max}$, $\rho_{d,min}$ of DL Cl and ASTM D 425 maximum dry unit we to a water content w weight $\rho_{d,max}$ was 10.4

(a) ISSS =

Fig. 7 Results from cyclic DSS test with initial static shear stress

(b) ISSS

0, 9.81, and 19.6 kPa were applied under a loading rate of 196.2 kPa/hr before cyclic loading, which did not exceed the peak shear stress τ_{peak} (namely equal to shear strength τ_f) of 27 kPa obtained from static tests. The static test was also performed under constant volume conditions in which the shear stress was applied under a constant strain rate of 0.1 %/min until reaching a shear strain of 20%. With the same rate of strain the ISSS was applied under constant stress conditions. On the other hand, for cyclic DSS tests, the cyclic shear stress $\tau_{f,cy}$ with stress control was applied to specimens under constant volume conditions, until either 50 cycles were reached or a 10% double amplitude shear strain $_{DA}$ was attained. The frequency of cyclic loading was 0.1 Hz for all of the tests.

The monotonic test was performed 10 min after the completion of the cyclic loading in order to allow the uniform distribution of excess pore water pressures, and the static shear stress was applied in the same manner as for the static test without previous cyclic loading.

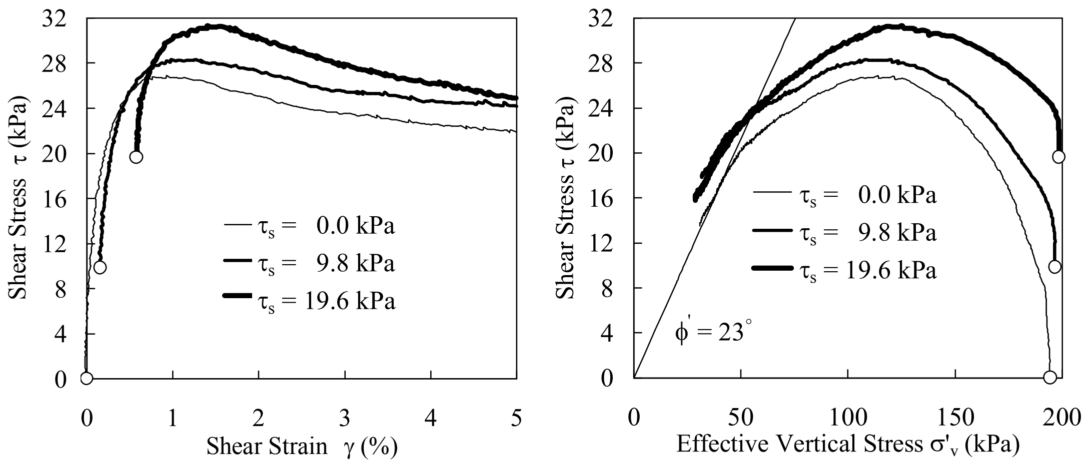

(a) Shear stress – shear strain

(b) Shear stress – effective vertical stress

Fig. 5 Static test results with initial static shear test

INFLUENCE OF INITIAL STATIC SHEAR STRESS ON MONOTONIC AND CYCLIC SHEAR STRENGTH AND STIFFNESS

Static Test

Figure 5 shows results of static or monotonic test on specimens with ISSS: those are shear stress – shear strain and effective vertical stress relations. From Fig. 5(a) it is known that the higher ISSS the specimen undergoes the larger shear strength is developed. This is probably caused by the fact that the volume in specimens decreases under the influence of ISSS. In Fig. 5(b) effective frictional angle ϕ' equal to 23° were determined. Since the DSS test apparatus is not able to measure pore pressures, it is calculated using the changes in vertical stresses observed during shear under the volume constant condition as was previously described. From Fig. 5 shear strength and maximum stiffness G_{max} from test with increasing ISSS can be drawn using the procedure as shown in Fig. 6(b). Figure 6(a) shows a definition of post-cyclic shear strength $_f$ and maximum stiffness G_{max}, and the results are showed in Fig. 6(b).

(b) ISSS =

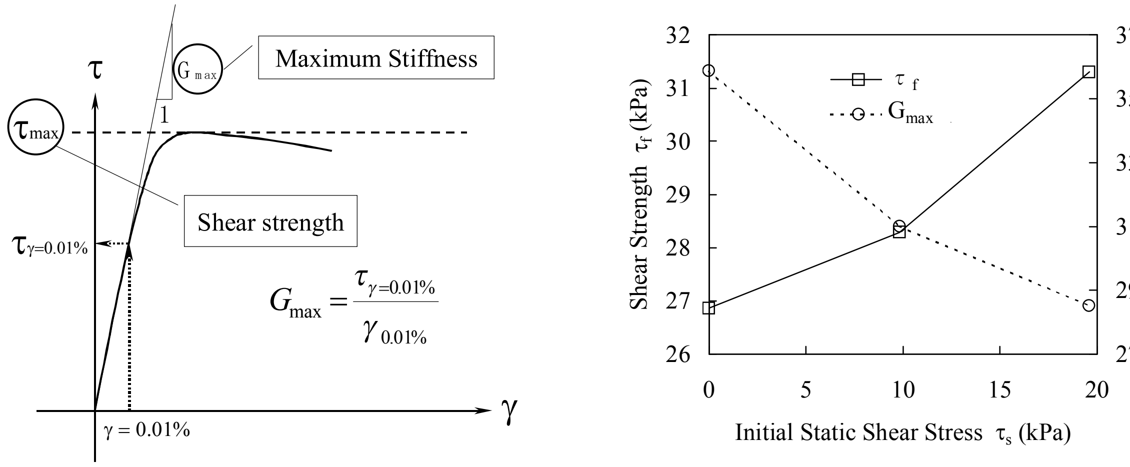

$$G_{max} = \frac{\tau_{\gamma=0.01\%}}{\gamma_{0.01\%}}$$

(c) ISSS = 19.

(a) Definition of shear strength and maximum stiffness

(b) Shear strength and maximum stiffness

Fig. 6 Shear strength and maximum stiffness from static DSS tests

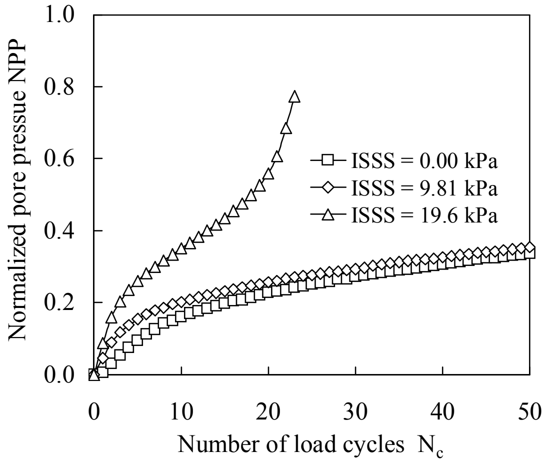

Fig. 8 Relation of normalized pore pressure vs. number of load cycles

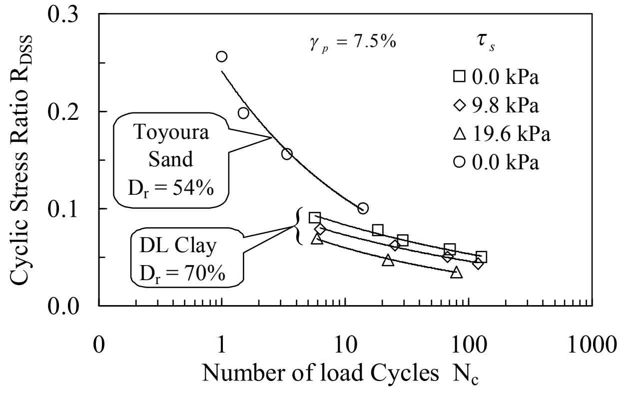

Fig. 10 Relation between cyclic ratio and number of load cycles

Cyclic Test

Figure 7 and 8 show a typical set of results from a family of cyclic DSS tests on specimens with three different ISSS. The applied cyclic stress ratio R_{DSS} is about 0.048 in this test. The cyclic stress ratio R_{DSS} is defined by:

$$R_{DSS} = \frac{\tau_{f,cy}}{\sigma'_{vc}} \tag{1}$$

where $\tau_{f,cy}$ is cyclic shear stress, and σ'_{vc} is effective vertical stress at applying a initial confined stress with consolidation pressure as $\sigma'_{v,,NCi}$ in Fig. 2. It is seen from Fig. 7 that the cyclic shear strain γ increases with increasing ISSS τ_s, while the vertical effective stress σ'_v decreases under the same cyclic shear stress. The shear strain in Fig. 7 (c) is larger than that in the other cases shown in Fig. 7 (a) and Fig. 7 (b). The reason for this tendency must be due to the fact that cyclic failure occurred due to the large cyclic shear stress $\tau_{f,cy}$ since the ISSS is larger than those in the cases of Fig. 7 (a) and (b).

Figure 8 shows an influence of ISSS on relations between normalized pore pressure NPP and number of load cycle N_c. The normalized pore pressure NPP is defined by:

$$NPP = \frac{\Delta u}{\sigma'_{vc}} = \frac{\sigma'_{vc} - \sigma'_{v}}{\sigma'_{vc}} \tag{2}$$

where Δu is excess pore pressure, and σ'_{vc} and σ'_v are the effective vertical stress before and after cyclic loading. Through Figs. 7 and 8 it can be seen that the influence of ISSS is not clear at the small ISSS, but in the case of large ISSS the shear strain γ and the normalized pore pressure NPP build up faster than that without ISSS.

Figure 9 shows the relations between normalized pore pressured NPP and number of load cycles N_c normalized by the number of load cycles N_{cl} at liquefaction. The solid line

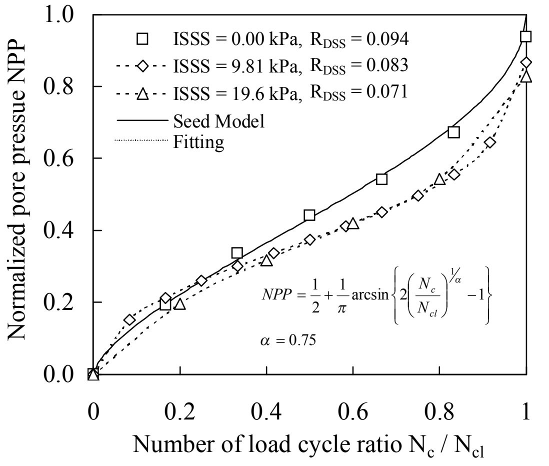

Fig. 9 Relation of normalized pore pressure vs. number of load cycle ratio

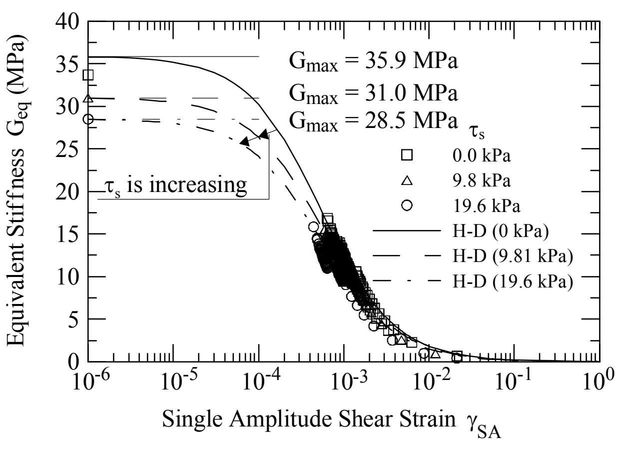

Fig. 11 Equivalent stiffness vs. single amplitude shear strain

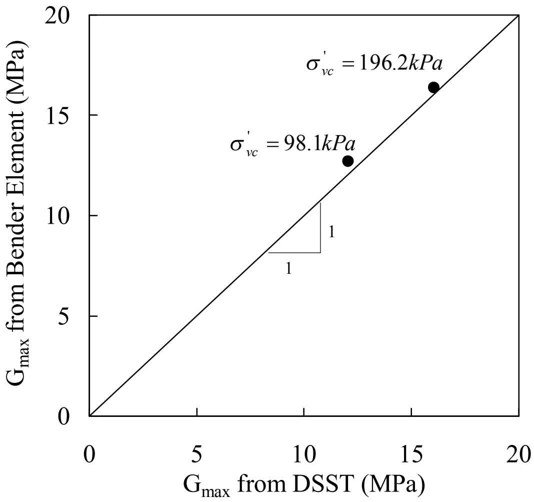

Fig. 12 Comparison between G_{max} from DSS test and bender element

calculated by following the relation proposed by Seed et al. (1975) as:

$$NPP = \frac{1}{2} + \frac{1}{\pi}\arcsin\left\{2\left(\frac{N_c}{N_{cl}}\right)^{1/\alpha} - 1\right\} \tag{3}$$

where α is 0.75 as a parameter is depending on the soil type. From cyclic DSS tests, it is clear that the relation between normalized pore pressure and number of load cycle ratio N_c /N_{cl} obtained without ISSS can be fitted by Eq. (3). Because Eq. (3) was developed for the results without ISSS, results with ISSS are not well matched with Eq. (3) even if the parameter is changed for the cases with ISSS. Therefore, a new model is needed to enable prediction of the normalized pore pressure NPP vs. number of load cycle ratio N_c /N_{cl} relation with ISSS.

CYCLIC-INDUCED DEGRADATION IN STRENGTH AND STIFFNESS

Figure 10 shows relation between cyclic stress ratio R_{DSS} and number of cycles N at peak shear strain γ_p = 10% in the cases with ISSS. The peak shear strain γ_p is taken from shear stress vs. shear strain relations with and without ISSS τ_s. The peak shear strain γ_p is used instead of a double shear strain γ_{DA} when there is no relation without ISSS. But the peak shear strain γ_p is employed when there is the relation with ISSS, because it is very difficult to get precisely a double shear strain γ_{DA} with ISSS (Vaid and Chern 1983; Hyodo et al. 1994). In Fig. 10 it is known that strength degradation happens with increasing ISSS τ_s. The cyclic stress ratio R_{DSS} vs. number of load cycle N_c curves for silt are compared with those for Toyoura Sand in which tests under the constant volume condition was conducted by using direct shear (DS) tests. Comparing with sand, non-plastic silt belongs to a very weak soil against cyclic loading even if the relative density of non-plastic silt is larger than that of sand.

Figure 11 shows the equivalent stiffness G_{eq} versus the single amplitude shear strain γ_{SA} relation indicating the initial values of G_{max} obtained by extrapolation of the Hardin-Drnevich (H-D) model (Hardin and Drnevich 1972). The equivalent stiffness or shear modulus G_{eq} was determined using (Vucetic et al. 1998):

$$G_{eq} = \frac{\tau_{max} - \tau_{min}}{\gamma_{max} - \gamma_{min}} \tag{4}$$

In Fig. 11 all the data for each cyclic loading step in cyclic tests was plotted. Introducing an empirical constant α to give three different lines modified the Hardin-Drnevich model. The reason for adapting this value was that were obtained by the Hardin-Drnevich model was not applied to silt but to sand. The modified Hardin-Drnevich model in the present paper is thus given by:

$$G_{eq} = \frac{G_{max}}{1 + \alpha(\gamma_{SA}/\gamma_r)} \tag{5}$$

where G_{max} is the maximum equivalent stiffness in static tests, γ_{SA} is single amplitude shear strain, γ_r is standard shear strain, and α is a empirical constant. Although the constant α is incorporated the modified Hardin-Drnevich model matches well with all the results from DSS tests on silt as can be seen in Fig. 11. The maximum stiffness G_{max} was determined by static shear tests (refer to Fig. 6). The constant α are 1.5, 1.6, and 2 corresponding to for the ISSS τ_s 0, 9.8, and 19.6 kPa, respectively.

To confirm a reliability of the results from DSS tests the maximum stiffness G_{max} from bender element was compared with that from DSS test in Fig. 12. From the tested results in Fig. 12 it is known that the maximum stiffness G_{max} from the static DSS test is almost the same as that obtained from the bender element. Maximum stiffness from the bender element can be calculated easily. As shown in Fig. 3(b), the shear wave is sent to a receiver from a transmitter. Elapsed time Δt of the shear wave can be known using the bender element. In Fig. 3(b) a distance h transferred can be taken between the top and the bottom of the bender element. The maximum stiffness G_{max} determined using the bender element is calculated by (Tanizawa et al. 1994):

$$G_{max} = \rho v_s^2 \tag{6}$$

$$v_s = h/\Delta t \tag{7}$$

where ρ is soil density, v_s is shear wave velocity, and Δt is the elapsed time of the shear wave.

DEGRADATION IN STRENGTH AND STIFFNESS OBSERVED FROM POST-CYCLIC DSS TESTS

Figure 13 shows a typical set of relations between shear stress versus shear strain and effective vertical stress in static, cyclic and post-cyclic tests on specimens with ISSS. Cyclic softening is commonly observed in the post-cyclic effective stress paths in Fig. 13. To show the influence of ISSS the results from cyclic DSS tests are compared using almost the similar cyclic stress ratio R_{DSS}. In Fig. 13 it is known that the excess pore pressure Δu is increased with increasing ISSS. The post-cyclic shear strength is increased with ISSS, but the larger ISSS is the smaller post-cyclic shear strength becomes. Figure 14 demonstrates that post-cyclic shear strength tends to decrease with increasing normalized pore pressure $\Delta u/\sigma'_{vc}$ for the all cases of ISSS.

Post-cyclic degradation of strength

Figure 15 shows the change in strength characteristics with and without ISSS τ_s after cyclic loading. In every case post-cyclic strength $\tau_{f,cy}$ is normalized by the static shear strength $\tau_{f,Nci}$ without cyclic loading obtained from the static DSS test (see Fig. 6). In Fig. 15 it is known that the shear strength $\tau_{f,cy}$ is increased with increasing ISSS τ_s.

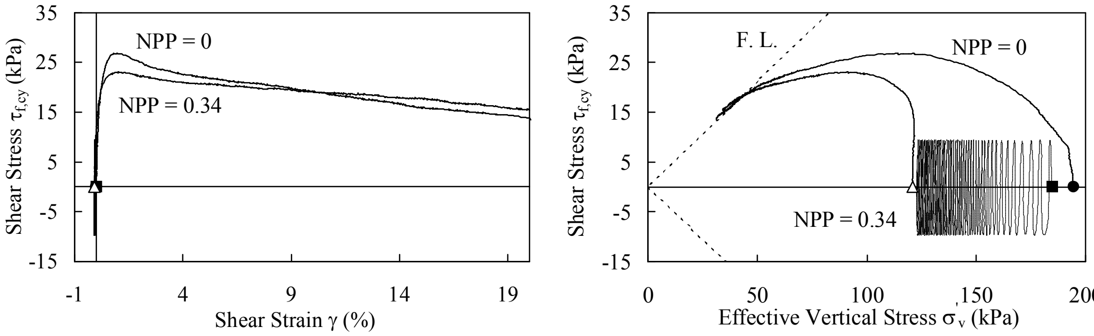

(a) ISSS = 0.0 kPa (R_{DSS} = 0.049)

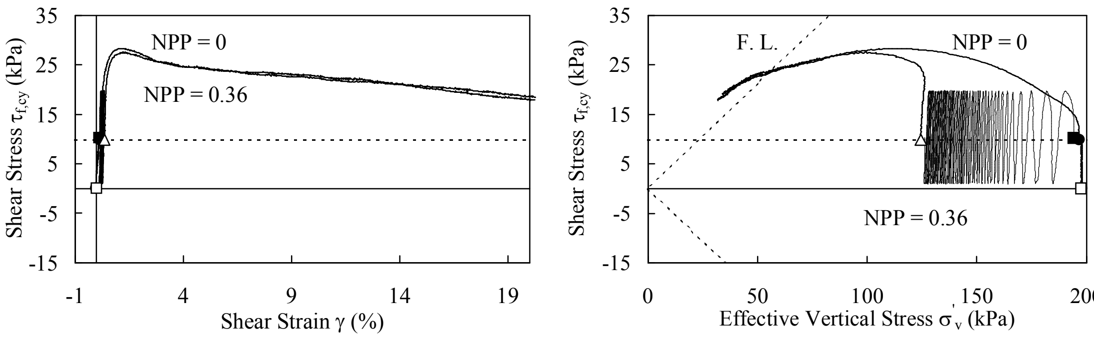

(b) ISSS = 9.8 kPa (R_{DSS} = 0.048)

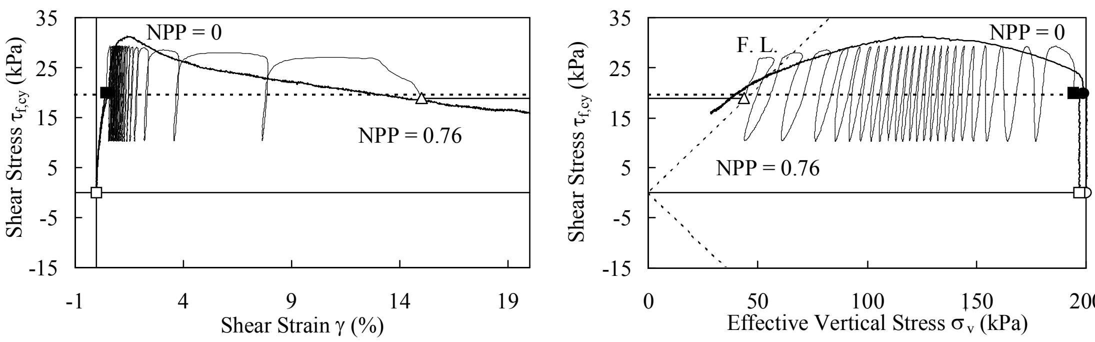

(c) ISSS = 19.6 kPa (R_{DSS} = 0.046)

Fig. 13 A set of static, cyclic and post-cyclic test results with ISSS

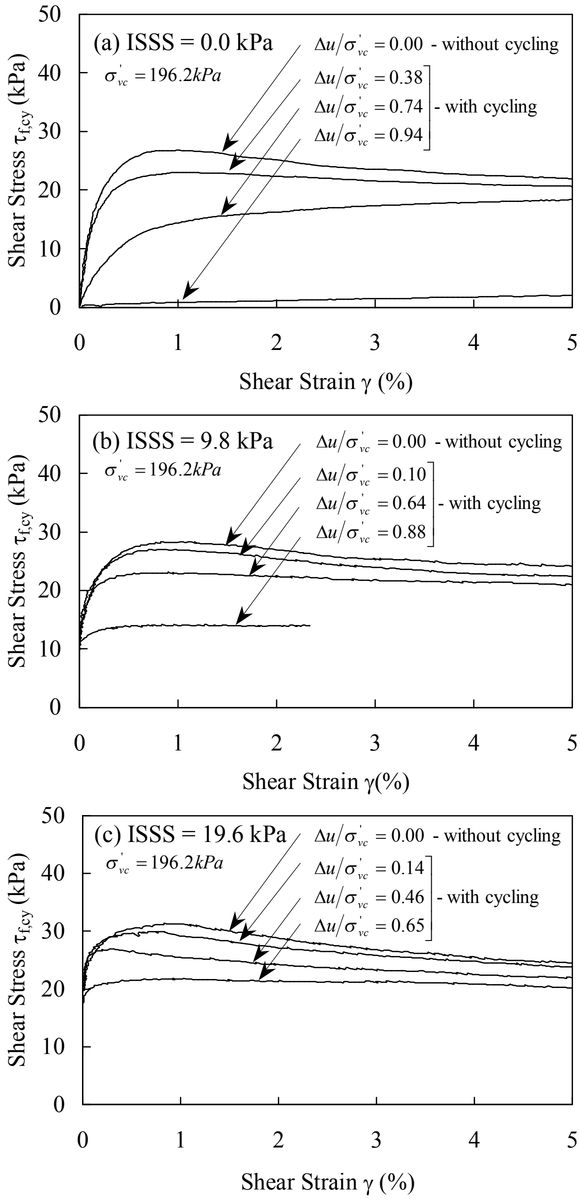

Fig. 14 Post-cyclic shear stress vs. shear strain

In Fig. 15(a), decrease of the strength ratio $\tau_{f,cy}$ / $\tau_{f,,NCi}$ with increasing cyclic load ratio R_{DSS} becomes rapid at a certain value of the cyclic stress ratio R_{DSS}. With increasing ISSS τ_s, the more marked decrease in the strength ratio $\tau_{f,cy}$ / $\tau_{f,NCi}$ starts at a lower value of the cyclic stress ratio R_{DSS}. Figure 15(b) shows that the strength ratio $\tau_{f,cy}$ / $\tau_{f,NCi}$ also decreases with increasing normalized pore pressure $\Delta u/\sigma'_{vc}$. Using the results from post-cyclic monotonic DSS tests post-cyclic degradation of strength for non-plastic silt is formulated into:

$$\frac{\tau_{f,cy}}{\tau_{f,NCi}} = \left(1 - A_1\left(\frac{\Delta u}{\sigma'_{v,NCi}}\right)\right)^{0.2} \exp\left(1.53\frac{\tau_s}{\sigma'_{v,NCi}}\right) \qquad (8)$$

where A_1 is a parameter to determine decreasing tendency of shear strength ratio $\tau_{f,cy}$ / $\tau_{f,,NCi}$, and the second order in Eq. (7) is expressed influence of ISSS τ_s from Fig. 6. The parameter A_1 is depended on ISSS τ_s like:

$$A_1 = 1.07\exp\left(0.63\frac{\tau_s}{\sigma_{v,NCi}}\right) \qquad (9)$$

This is slightly different from the proposal by Yasuhara (1985, 1994b) and Yasuhara et al. (1992) for predicting post-cyclic undrained strength of cohesive soils using triaxial tests.

Post-cyclic degradation of stiffness

Figure 16 shows the change in stiffness characteristics with and without ISSS τ_s after cyclic loading. In every case post-cyclic stiffness G_{cy} is also normalized by the stiffness G_{NCi} obtained from the static test (Fig. 6). As well as Fig.15(a), Fig. 16(a) indicates that the slope of the degradation of the stiffness ratio $G_{max,cy}$ / $G_{max, NCi}$ with

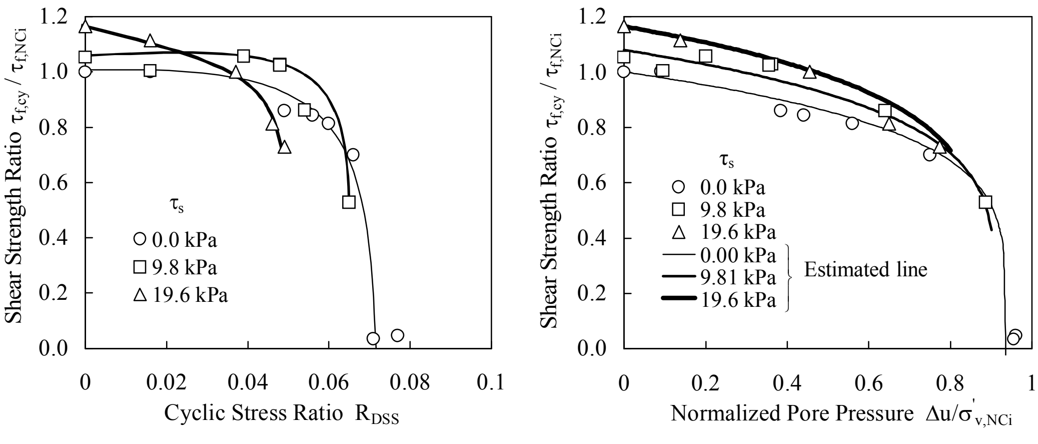

(a) Shear strength ratio vs. cyclic stress ratio (b) Shear strength ratio vs. normalized pore pressure

Fig. 15 Post-cyclic induced degradation of strength

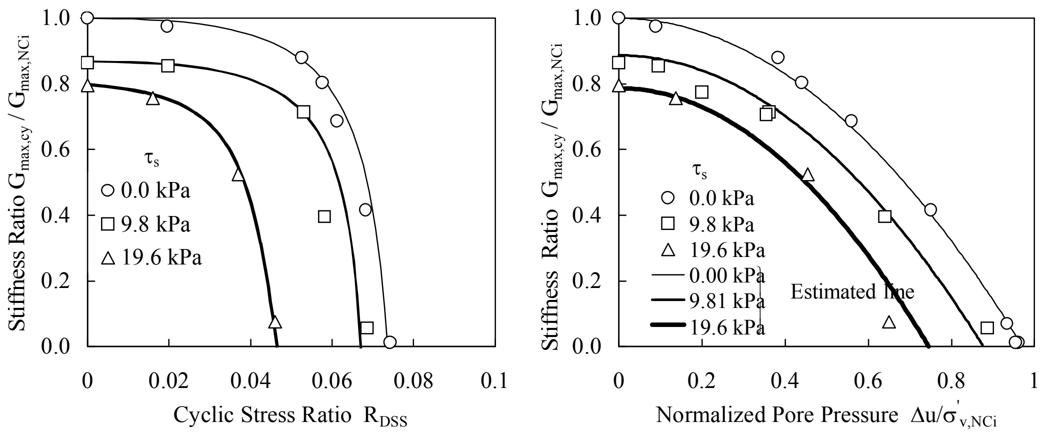

(a) Stiffness ratio vs. cyclic stress ratio (b) Stiffness ratio vs. normalized pore pressure

Fig. 16 Post-cyclic induced degradation of stiffness

increasing cyclic load ratio R_{DSS}, rapidly increases at a certain value of the cyclic stress ratio R_{DSS}. With increasing ISSS τ_s, the more rapid decrease in the stiffness ratio $G_{max,cy}$ / $G_{max,\,NCi}$ is observed at a lower value of the cyclic load ratio R_{DSS}. From Fig. 16(b) showing the stiffness ratio $G_{max,cy}$ / $G_{max,\,NCi}$ and normalized pore water pressure Δu / $\sigma'_{v,NCi}$ relations, it is also clear that the stiffness ratio $G_{max,cy}$ / $G_{max,\,NCi}$ decreases with increasing normalized pore pressure Δu / $\sigma'_{v,NCi}$. Using results tested the post-cyclic degradation of stiffness for non-plastic silt is estimated as:

$$\frac{G_{cy}}{G_{NCi}} = \left(1 - A_2\left(\frac{\Delta u}{\sigma'_{v,NCi}}\right)^2\right)\exp\left(-2.3\frac{\tau_s}{\sigma'_{v,NCi}}\right) \tag{10}$$

where A_2 is a parameter to determine decreasing tendency of stiffness ratio $G_{max,cy}$ / $G_{max,\,NCi}$, and the second order in Eq. (9) shows an influence of ISSS τ_s formulated from Fig. 6 and is given as:

$$A_2 = 1.04\exp\left(5.23\frac{\tau_s}{\sigma_{v,NCi}}\right) \tag{11}$$

As well as Eq. (7), Eq(9) is also different from the relation proposed by Yasuhara et al. (1994a, 1997, 1998). However, it is the same form as the relation proposed by Shimabukuro et al. (2000), which is valid for post-cyclic stiffness prediction of non-plastic silt in triaxial tests.

By comparing Figs. 15 with 16 it is concluded that post-cyclic degradation of strength and stiffness shows similar tendencies with each other. Also, the tendency of the strength ratio $\tau_{f,cy}$ / $\tau_{f,,NCi}$ and the stiffness ratio $G_{max,cy}$ / $G_{max,\,NCi}$ tends to decrease similarly when those are plotted against the cyclic load ratio R_{DSS} and the normalized pore pressure Δu / $\sigma'_{v,NCi}$.

CONCLUSION

In this paper, the post-cyclic strength and stiffness degradation of non-plastic silt was investigated using direct simple shear (DSS) tests. It was found that the strength and stiffness of non-plastic silt after liquefaction almost disappeared in the cases without initial static shear stress (ISSS). On the other hand, even if it was very difficult to determine the shear strength and stiffness of non-plastic silt with ISSS after cyclic loading, it was carefully investigated. The following are the main conclusions derived from the present study:

1) Cyclic and post-cyclic degradation of non-plastic silt is very sensitive to the application of ISSS. In particular, degradation in stiffness is more sensitive to ISSS than that in strength.

2) Both the strength and the stiffness to the normalized pore pressure decrease markedly with increasing ISSS.

3) Through the results from cyclic DSS tests on non-plastic silt, characteristics of post-cyclic degradation in strength and stiffness should depend on the fact that the generation of pore pressures during cyclic loading is marked with increasing ISSS.

4) Using the results from post-cyclic DSS tests, post-cyclic degradation relations for strength and stiffness for non-plastic silt are formulated against cyclically induced excess pore pressure. The effect of ISSS is included in these proposed relations.

ACKNOWLEDGEMENT

The author appreciates to Prof. Yasuhara, Associate Prof. Komine, and Research Associate Murakami in Ibaraki Univ. for their advice and encouragement on this research.

REFERENCES

Andersen, K.H., Brown, S.F., Foss, I., Pool, J.H., and Rosenbrand, W.F. 1976. Effect of cyclic loading on clay behaviour. Proc. Conf. on Design and Construction of Offshore Structures, Inst. Civ. Engrs: 75-79.

Aydan, Ö., Ulusay, R., Hasgür, Z. and Taskin, B. (2000). A Site Investigation of Kocaeli Earthquake of August, 17, 1999. Turkish Earthquake Foundation, TDV/DR 08-49, URL: http://www.princeton.edu/~mcakir/deprem/kocaeli/kocaelicontent.html, Department of Operations Research and Financial Engineering, Princeton, USA, 31 March 2000.

Bjerrum, L., and Landva, A. (1966). Direct Simple-Shear Test on a Norwegian Quick Clay. Geotechnique. 16(1): 1-20.

Hamada, M., Tohma, J., and Aydan, Ö. (1999). The 1999 Kocaeli Earthquake, Turkey – Investigation into the Damage to Civil Engineering Structures. Japanese Society of Civil Engineering. URL : http://www.jsce.or.jp/report/index.html, JSCE, Tokyo, Japan, 12 Dec. 2001.

Hardin, B. O. and Drnevich, V. P. (1972). Shear Modulus and Damping in Soils: Design Equations and Curves. J. Soil Mech. and Foundations Division, ASCE. 98(7): 667-692.

Head, K. H. (1992). Manual of soil Laboratory Testing, Vol. 1, Soil Classification and Compaction Tests, 2nd edition, Pentech press, London.

Hyodo, M., Tanimizu, H. Yasufuku, N. and Murata, H. (1994). Undrained cyclic and monotonic triaxial behaviour of saturated loose sand. Soils and Foundations. 34(1). 19-32.

Japanese Geotechnical Society. (1993). From Investigation and Design to Construction for Countermeasure of Liquefaction – Soil and Foundation Series for Engineer. Japanese Geotechnical Society.

Japanese Geotechnical Society. (2000a). Reports on the investigations of the 1999 Kokaeli Earthquake in Turkey and the 1999 Chichi Earthquake in Taiwan. Japanese Geotechnical Society. CD-Rom (in Japanese).

Japanese Geotechnical Society. (2000b). Reports on the investigations of the 2000 Tottoriken-Seibu Earthquake in Japan. Japanese Geotechnical Society. CD-Rom (in Japanese).

Japanese Geotechnical Society. (2000c). The Method of Soil Test and Explanation (the 1st Edition). Japanese Geotechnical Society (in Japanese).

Seed, H. B., Martin, P. P. and Lysmer, J. (1975). The generation and dissipation of pore pressures during soil liquefaction. Earthquake Engineering Research Center, Report No. UCB/EERC 75-26.

Shimamoto, E., Numata, A., Someya N., Miwa S., Ikeda T., and Ohno K. (2001). Liquefaction during the 2000 Tottori-ken Seibu Earthquake. The 36th Japan National Conference on Soil Mech. and Foundation Eng., Tokushima, Japan. Vol. 2: 2149-2150 (in Japanese).

Shimabukuro, A., Yasuhara, K., and Murakami, S. (2000). Effect of sample preparation on liquefaction and post-liquefaction characteristics of a non-plastic silt. JSCE. III-52(659): 39-49 (in Japanese).

Tanizawa, F., Teachavorasinskun, S., Yamaguchi, J., Sueoka, T., and Goto, S. (1994). Measurement of shear wave velocity of sand before liquefaction and during cyclic mobility. Proc. Int. Sym. Pre-failure deformation of geomaterials, Sapporo, Japan. Vol.1 : 63-68.

Vaid, Y. P. and Chern, J. C. (1983). Effect of static shear on resistance to liquefaction. Soils and Foundations. 23(1). 47-60.

Vucetic, M., Lanzo, G., and Doroudian, M. (1998). Damping at Small Strains in Cyclic Simple Shear Test. J. Geotechnical and Geoenvironmental Eng., ASCE. 124(7): 585-594.

Yasuhara, K. (1985). Undrained and Drained Cyclic Triaxial Tests on a Marine Clay. Proc. the 11th ICSMFE, San Francisco, USA, Vol. 2.: 1095-1098.

Yasuhara, K. (1994a). Method for estimating postcyclic undrained secant modulus of clays. Geotech. and Geoenv. Eng., ASCE. 123(3): 204-211.

Yasuhara, K. (1994b). Postcyclic Undrained Strength for Cohesive Soils. J. Geotech. and Geoenv. Eng., ASCE. 120(11): 1961-1979.

Yasuhara, K. and Nagano, M. (1995). Post-Cyclic Behavior of Clay in Direct Shear Tests. Proc. 10th Asian Regional Conf. on SMFE, Beijing, China, Vol. 1: 119-122.

Yasuhara, K., Fujiwara, H., Hirao, K., and Ue, S. (1983). Undrained Shear Behavior of Quasi-overconsolidated Clay Induced by Cyclic Loading. Proc. IUTAM Symp., Seabed Mech., Newcastle Upontyne, UK.: 17-24.

Yasuhara, K., Hirao, K., and Hyde, A. F. L. (1992). Effects of Cyclic Loading on Undrained Strength and Compressibility of Clay. J. Japanese Society of Soil Mechanic and Foundations Engineering. 32(1): 100-116.

Yasuhara, K., Hyde, A F L, Toyota, N. and Murakami, S. (1998). Cyclic Stiffness of Plastic Silt with an Initial Drained Shear Stress. Geotechnique, Special Issue on Pre-failure Deformation Behaviour of Geomaterials: 373-382.